

# A Quantitative Model for the In Vivo Assessment of Drug Binding Sites with Positron Emission Tomography

Mark A. Mintun, MD,\*‡ Marcus E. Raichle, MD,\*†‡ Michael R. Kilbourn, PhD,\*  
G. Frederick Wooten, MD,‡§ and Michael J. Welch, PhD\*

We propose an in vivo method for use with positron emission tomography (PET) that results in a quantitative characterization of neuroleptic binding sites using radiolabeled spiperone. The data are analyzed using a mathematical model that describes transport, nonspecific binding, and specific binding in the brain. The model demonstrates that the receptor quantities  $B_{\max}$  (i.e., the number of binding sites) and  $K_D^{-1}$  (i.e., the binding affinity) are not separably ascertainable with tracer methodology in human subjects. We have, therefore, introduced a new term, the binding potential, equivalent to the product  $B_{\max}K_D^{-1}$ , which reflects the capacity of a given tissue, or region of a tissue, for ligand-binding site interaction. The procedure for obtaining these measurements is illustrated with data from sequential PET scans of baboons after intravenous injection of carrier-added [ $^{18}\text{F}$ ]spiperone. From these data we estimate the brain tissue nonspecific binding of spiperone to be in the range of 94.2 to 95.3%, and the regional brain spiperone permeability (measured as the permeability-surface area product) to be in the range of 0.025 to 0.036  $\text{cm}^3/(\text{s} \cdot \text{ml})$ . The binding potential of the striatum ranged from 17.4 to 21.6; these in vivo estimates compare favorably to in vitro values in the literature. To our knowledge this represents the first direct evidence that PET can be used to characterize quantitatively, locally and in vivo, drug binding sites in brain. The ability to make such measurements with PET should permit the detailed investigation of diseases thought to result from disorders of receptor function.

Mintun MA, Raichle ME, Kilbourn MR, Wooten GF, Welch MJ: A quantitative model for the in vivo assessment of drug binding sites with positron emission tomography. *Ann Neurol* 15:217-227, 1984

Various radioligands have been used widely in post-mortem and in vitro experiments to characterize drug binding sites or receptors in the central nervous system of experimental animals and humans in relation to a variety of diseases [1, 4, 5, 8, 18-20]. These methods are inadequate for correlating the natural history of diseases with in vivo changes in drug binding sites, however. It has often been claimed that positron emission tomography (PET) will provide the means to perform in vivo quantitative receptor analysis [23], but no quantitative in vivo radiotracer method has emerged that serves this function.

The challenge to PET is not only to provide, as it can [23], in vivo evidence of the local accumulation of a specific radioligand, but also to yield quantitative estimates of specific features of the binding sites, such as their number and affinity. However, the exact in vivo distribution of such a radioligand at a single time point is likely to be influenced by a variety of factors besides the number of receptors and their affinity. These in-

clude binding to nonspecific sites, blood-brain barrier permeability, and blood flow. The approach of the pharmacologist attempting to minimize these influences traditionally has been to isolate the tissue of interest in vitro and to manipulate the binding of the radioligand by occupying the binding sites or receptors with varying concentrations of the ligand (unlabeled), other unlabeled drugs, or putative transmitters. In this way the pharmacologist extracts quantitative estimates of the number of binding sites and their affinity. Such manipulations usually involve very high concentrations of drugs at the receptor site and therefore would not be appropriate for in vivo studies in human subjects because of the unwanted pharmacological side effects. If PET is to achieve quantitative measurements of the number of drug binding sites and their affinity, some approach not involving the classic displacement studies of the pharmacologist must be developed. The most obvious alternate approach is to utilize the potential of PET to make repeated measurements of local radioac-

From the \*Edward Mallinckrodt Institute of Radiology, the †McDonnell Center for Studies of Higher Brain Function, and the ‡Department of Neurology and Neurosurgery (Neurology), Washington University School of Medicine, St Louis, MO 63110.

Received Nov 5, 1982, and in revised form June 3 and Aug 2, 1983. Accepted for publication Aug 11, 1983.

§Present address: Department of Neurology, University of Virginia Medical Center, Charlottesville, VA 22908.

Address reprint requests to Dr Raichle, Washington University School of Medicine, Box 8131, St Louis, MO 63110.

tivity in the same tissue, thus characterizing the dynamic interplay between binding site and ligand, and to combine these measurements in the same subject at the same sitting with the measurement of other important features of the tissue, such as local blood flow, blood-brain barrier permeability, and blood volume. Effectively utilizing this potential of PET requires the formulation of a detailed mathematical model that provides the investigator with the proper framework within which to develop a measurement strategy in humans using PET. Toward this goal we propose an in vivo method that results in quantitative characterization of regional drug binding sites in vivo. The method uses radiolabeled spiperone (a potent butyrophenone), a quantitative mathematical model to describe the drug's behavior in the brain, and sequential PET scans for in vivo data acquisition. To illustrate our quantitative receptor model we have used baboons injected with fluorine 18-labeled spiperone ( $[^{18}\text{F}]$ spiperone) and multiple PET scans to collect profiles of brain tissue activity.

## Methods

### Model

Schemata and symbols of our model are shown in Figure 1 and Table 1, respectively.

The model chosen assumes three possible environments for spiperone, and thus requires three mathematical compartments. The first two are physical compartments representing blood and brain tissue. The third compartment represents a chemical environment, i.e., being bound to a specific binding site. In this compartment spiperone is physically in the tissue but not free to diffuse until it leaves this environment by dissociating from the binding site.

For a given model volume spiperone may enter via arterial blood flow into the blood compartment. It is assumed that all compartments are homogeneous in concentration; thus, the spiperone departs from the blood compartment through venous drainage at a concentration equal to that of the blood compartment. Spiperone may cross the blood-brain barrier into the tissue compartment by passive linear diffusion. Only in the tissue compartment is it free to react with drug binding sites according to classic kinetics: bimolecular association and unimolecular dissociation. Additionally, there are nonspecific, nonsaturable spiperone binding sites in both blood and tissue compartments. The quantity of drug free to diffuse or react with binding sites is represented by the total drug concentration multiplied by a constant, the free fraction ( $f_i$ ).

The differential equation set that describes the drug's behavior in brain is developed by first writing the conservation equation for each compartment. For the  $i$ th compartment:

$$V_i \cdot \frac{dC_i}{dt} = \Phi_{i,\text{in}} - \Phi_{i,\text{out}}$$

where  $\Phi_{i,\text{in}}$  and  $\Phi_{i,\text{out}}$  are the fluxes in and out of this compartment.

The fluxes are then defined. Note that convective terms

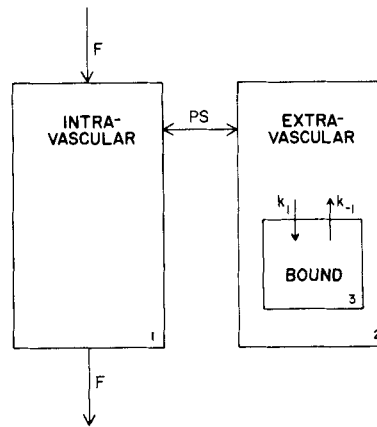


Fig 1. Three-compartment model used in analysis of brain tissue data obtained after intravenous injection of ( $^{18}\text{F}$ )spiperone. Compartments 1, 2, and 3 represent the possible environments for the radioligand. Interactions between compartments are governed by variables for convection ( $F$ ), diffusion ( $PS$ ), and binding kinetics ( $k_{-1}$ ,  $k_1$ ).

include the  $F$  parameter, diffusion terms include  $PS$ , and specific binding terms include  $k_1$  or  $k_{-1}$ . The arterial blood concentration is represented by  $C_A$ . Additionally, the number of free specific binding sites is expressed as the total binding site concentration minus the concentration bound.

$$\begin{aligned} \Phi_{1\text{in}} &= F \cdot C_A + PS \cdot f_2 \cdot C_2 \\ \Phi_{1\text{out}} &= F \cdot C_1 + PS \cdot f_1 \cdot C_1 \\ \Phi_{2\text{in}} &= PS \cdot f_1 \cdot C_1 + k_{-1} \cdot C_3 \cdot V_2 \\ \Phi_{2\text{out}} &= PS \cdot f_2 \cdot C_2 + k_1 \cdot C_2 \cdot f_2 \cdot (B_{\text{max}} - C_3) \cdot V_2 \\ \Phi_{3\text{in}} &= k_1 \cdot C_2 \cdot f_2 \cdot (B_{\text{max}} - C_3) \cdot V_2 \\ \Phi_{3\text{out}} &= k_{-1} \cdot C_3 \cdot V_2 \end{aligned}$$

Substituting the expressions for flux into the conservation equations for compartments 1, 2, and 3, we can then write the complete differential equation set.

$$\begin{aligned} \frac{dC_1}{dt} &= \frac{F}{V_1} (C_A - C_1) + \frac{PS}{V_1} (f_2 C_2 - f_1 C_1) \\ \frac{dC_2}{dt} &= \frac{PS}{V_2} (f_1 C_1 - f_2 C_2) + k_{-1} \cdot C_3 - k_1 \cdot f_2 \cdot C_2 \\ &\quad \cdot (B_{\text{max}} - C_3) \\ \frac{dC_3}{dt} &= k_1 \cdot f_2 \cdot C_2 \cdot (B_{\text{max}} - C_3) - k_{-1} \cdot C_3 \end{aligned}$$

Eq. set 1

However, if one considers the ideal of tracer methodology, where the specific activity of the radioligand is sufficiently high that the molar quantities of ligands injected are vanishingly small, then the model equations need to be simplified. In this case the absolute value of  $C_3$  would always be much less than  $B_{\text{max}}$ , and thus  $(B_{\text{max}} - C_3)$  would reduce to  $(B_{\text{max}})$ . Substituting this term into Eq. set 1, we find that the  $B_{\text{max}}$  and  $k_1$  terms are no longer independent variables and can be replaced by a unimolecular rate constant  $k'_1$  where  $k'_1 = B_{\text{max}} \cdot k_1$ . This second substitution creates Eq. set 2, which is for use with low molar quantities of injected ligand.

$$\frac{dC_1}{dt} = \frac{F}{V_1} (C_A - C_1) + \frac{PS}{V_1} (f_2 C_2 - f_1 C_1)$$

Table 1. Variables Used in the Drug Binding Model<sup>a</sup>

Symbol	Description	Units
$V_i$	Volume of compartment $i$	ml
$C_i$	Drug concentration in compartment $i$	$\mu\text{Ci} \cdot \text{ml}^{-1}$
$f_i$	Drug fraction free from nonspecific binding	None
$F$	Regional blood flow	$\text{ml} \cdot \text{sec}^{-1}$
$PS$	Drug permeability of blood-brain barrier $\times$ capillary surface area	$\text{cm}^3 \cdot \text{sec}^{-1}$
$k_{-1}$	Reverse rate constant	$\text{sec}^{-1}$
$k_1$	Forward rate constant	$\text{ml} \cdot \text{sec}^{-1} \cdot \mu\text{Ci}^{-1}$
$B_{\text{max}}$	Maximum drug specific binding concentration	$\mu\text{Ci} \cdot \text{ml}^{-1}$
$k'_1$	Combined forward rate constant ( $k_1 \cdot B_{\text{max}}$ )	$\text{sec}^{-1}$
$BP$	Binding potential of specific binding	None

<sup>a</sup>Operationally, a total tissue volume of 1.0 ml is assumed when estimating parameter values.

$$\frac{dC_2}{dt} = \frac{PS}{V_2} (f_1 C_1 - f_2 C_2) + k_{-1} \cdot C_3 - k'_1 \cdot f_2 \cdot C_2$$

$$\frac{dC_3}{dt} = k'_1 \cdot f_2 \cdot C_2 - k_{-1} \cdot C_3$$

Eq. set 2

For both equation sets the average concentration of drug ( $C_{\text{tot}}$ ) in the total volume of tissue ( $V_{\text{tot}}$ ) is defined as

$$C_{\text{tot}} = \frac{[C_1 \cdot V_1 + V_2 \cdot (C_2 + C_3)]}{V_{\text{tot}}}$$

A value of 1.0 ml is assigned to  $V_{\text{tot}}$  as the unit model volume.

### Analysis of Data

The model Eq. set 1 involves a total of nine parameters:  $V_1$ ,  $V_2$ ,  $f_1$ ,  $f_2$ ,  $F$ ,  $PS$ ,  $k_{-1}$ ,  $k_1$ , and  $B_{\text{max}}$ . Eq. set 2 uses only eight parameters, as the last two are replaced with  $k'_1$ . In either set, four parameters are given values prior to data analysis. The tissue space that is available to the radioligand,  $V_2$ , is assumed equal to the tissue water space and has a value of  $0.76 \text{ ml} \cdot \text{g}^{-1}$  [13] or  $0.79 \text{ ml}$  for  $1 \text{ ml}$  of tissue (assuming a tissue density of  $1.05 \text{ g} \cdot \text{ml}^{-1}$ ). The parameter  $f_1$ , representing the fraction not bound to nonspecific sites in blood, can be measured with in vitro techniques and considered constant. The value used was 0.10 (i.e., 90% bound), an estimate supplied by Janssen Pharmaceutica (personal communication, 1981). The parameters for blood flow,  $F$ , and blood volume,  $V_1$ , are uniquely determined regionally by existing PET methods [9, 11, 25].

Because it is very difficult to estimate the values of all the remaining parameters simultaneously, we have chosen a method that accomplishes this in two distinct steps. Both steps use the techniques of numerical integration, curve-fitting, and parameter estimation, as we will describe.

The first step in data analysis obtains the  $PS$  and  $f_2$  parameters from cerebellum tissue data. The cerebellum is devoid of specific spiperone binding sites [17, 19]. Thus, for the cerebellum the model can be reduced in complexity by removing the specific binding site compartment. Once determined, the  $f_2$  value is assumed to be regionally constant and can be used in other areas of the brain, including areas rich in specific binding sites.

The equation set used to model the cerebellum with no specific binding sites is:

$$\frac{dC_1}{dt} = \frac{F}{V_1} (C_A - C_1) + \frac{PS}{V_1} (f_2 C_2 - f_1 C_1)$$

$$\frac{dC_2}{dt} = \frac{PS}{V_2} (f_1 C_1 - f_2 C_2)$$

Eq. Set 3

The second step in data analysis obtains the local  $PS$  and receptor terms from the tissue data in the area of interest. The actual terms estimated depend on the equation set chosen. If large molar doses of ligand are injected and partial saturation of specific sites is expected, Eq. set 1 could be selected, yielding estimates of  $PS$ ,  $k_{-1}$ ,  $k_1$ , and  $B_{\text{max}}$ . For small doses, when partial saturation will be absent, Eq. set 2 is appropriate, yielding  $PS$ ,  $k'_1$ , and  $k_{-1}$ . If Eq. set 1 is used when small doses of ligand are administered, the result will be an obvious nonunique set of solutions for  $k_1$  and  $B_{\text{max}}$ . Procedurally, all data are processed by Eq. set 1, and when nonunique solution sets are encountered, the data are then processed with Eq. set 2.

Results of data analysis with Eq. set 1 are expressed as  $B_{\text{max}}$  and  $K_D$ , where  $K_D = k_{-1}/k_1$ . Results of data analysis with Eq. set 2 are expressed with a term we have named the *binding potential (BP)*, where  $BP = k'_1/k_{-1} = B_{\text{max}} \cdot k_1/k_{-1} = B_{\text{max}} \cdot K_D^{-1}$ . Because of its derivation this term reflects the capacity of the tissue for ligand-binding site interaction. Of interest is that a mathematically similar term, the binding index, equal to the product of site concentration and affinity, is used to describe low-affinity, nonspecific binding in in vitro settings [6].

### Integration of Model Equations

To be useful in parameter estimation schemes, the operational equations must be integrated and rewritten to give concentrations as a function of time. Unfortunately, Eq. set 1 is nonlinear because of the bimolecular association terms and thus cannot be integrated analytically. The best alternate approach available is numerical integration, a computation-intensive procedure. The Runge-Kutta method [3] was selected for all three equation sets because of its simplicity (single-step formula, no partial derivatives) and high accuracy relative to biological data. All programming was done in Fortran and executed on a Perkin Elmer 32/42 minicomputer.

### Curve-fit Analysis

Curves of tissue activity versus time generated by numerical integration were evaluated for "closeness of fit" to biological data. The result was a single relative value found by summing the squares of the difference between predicted and observed tissue activity. All tissue points were given equal weight. Relative error =  $\sum_i (C_{obs} - C_{calc})$  for a given parameter set. The lower the relative error, the better the "fit" to observed data.

### Parameter Estimation

For any given parameter set and tissue activity data, the numerical integration and curve-fit analysis routines would result in a relative error.

Rosenbroch's rotating coordinate optimization technique [32] was used to find the parameter set that minimized the relative error. This method combines a direct-search algorithm using variable step sizes with a periodic rotation of search coordinates to point along the direction of the latest ridge. Although in the past we have used simpler techniques, such as the gradient method [2], we found that given the nature of the equations and the length of time necessary to do each numerical integration, the rotating coordinate method was very useful in minimizing the number of trials and considerably reducing computation time. Currently, optimum parameter solution is found after 20 to 120 minutes of computer time.

### Simulations

The estimates of  $PS$ ,  $f_2$ ,  $k_{-1}$ , and  $BP$  are clearly dependent on a number of factors. To understand more easily the nature of this dependence, we used model equation sets 2 and 3 in simulations designed to isolate and examine the error introduced by small errors in  $F$ ,  $V_1$ ,  $f_1$ ,  $PS$ , and  $f_2$ .

For all simulations the actual blood activity curve obtained from one of the animal studies was used (baboon 1; see this page), as well as the same PET scan times. The simulations all use Eq. sets 2 and 3, because these sets proved most applicable to the animal data collected.

To measure the effect of errors in the parameters  $F$ ,  $V_1$ ,  $V_2$ , and  $f_1$  on the calculation of  $PS$  and  $f_2$  (for cerebellum) or  $PS$ ,  $k_{-1}$ ,  $k'_1$ , and  $BP$  (for striatum), a tissue activity curve was first generated using the model equations and assuming a set of values for all parameters (the values assumed being comparable to those used or determined in this experimental work). A +5% error was then introduced into one of the parameters  $F$ ,  $V_1$ ,  $V_2$ , or  $f_1$  and, using this new value, the  $PS$  and  $f_2$  or  $k_{-1}$ ,  $k'_1$ , and  $BP$  were reestimated. The parameters were compared and the results expressed as percentage of error incurred.

The estimation of  $k_{-1}$ ,  $k'_1$ , and  $BP$  depend not only on external parameters, as noted, but on an internally calculated parameter,  $f_2$ . To calculate this dependence, the described technique was repeated, except that the +5% error was introduced into the  $f_2$  parameter. The values of  $k_{-1}$ ,  $k'_1$ , and  $BP$  were calculated and compared, with results expressed as percentage of error incurred.

### Positron Emission Tomography

The PETT VI system, a positron emission scanner developed at Washington University [28, 33], was employed for all

studies. Studies were done in the low-resolution mode, giving an in-plane (transverse) resolution of 11.7 mm full width at half maximum (FWHM). Data were recorded simultaneously from seven slices, each with a 15.9 mm FWHM thickness and a center-to-center slice separation of 14.4 mm.

The PETT VI system does not correct for radioactive decay during data collection, and it is necessary to correct all reconstructed scan data from patients or phantoms for the radioactive isotope decay during the study. We employ a method that assumes the underlying activity is reasonably constant and decay correction can be achieved with an "average" decay correction. This is computed as:

$$\begin{aligned} \text{average decay} &= \int_0^T \frac{\exp(-\alpha t) dt}{T} \\ &= \frac{1 - \exp(-\alpha T)}{T \cdot \alpha} \end{aligned}$$

where  $\alpha$  is the decay constant and  $T$  is the length of the scan. Inversion of this average decay yields the decay correction factor. Simulations (P. Herscovitch and M. E. Raichle, unpublished observations, 1981) of various functions equivalent to time-varying head activity curves likely to be encountered during our studies demonstrate that this method of decay correction is quite adequate (maximum error less than 4%).

Calibration of the PETT VI system to permit expression of findings of regional tissue activity is achieved by imaging a phantom containing various concentrations of carbon 11-labeled bicarbonate. Aliquots from each of the six wedge-shaped chambers are counted in the same well counter used to count the blood samples. The observed counting rate is decay corrected to the time the calibration scan begins and is then multiplied by the length of the scan. Results are expressed in counts  $\cdot \text{ml}^{-1}$ . By means of a regression equation, the reconstructed regional data (PET counts  $\cdot \text{pixel}^{-1}$ ) of the phantom are compared with the directly measured activity (counts  $\cdot \text{ml}^{-1}$ ). This relationship is used to calculate actual integrated local isotope tissue activity levels. This value is divided by the scan length to give average tissue activity level and assigned a time value equal to the midpoint of the scan.

Our method used to measure local cerebral blood flow (CBF) and blood volume (CBV) with oxygen 15-labeled water and PET, adapted from Kety [14, 15], is described elsewhere [11, 25], as is our method for measurement of cerebral blood volume using oxygen 15-labeled carbon monoxide [9].

In baboon studies using [ $^{18}\text{F}$ ]spiperone, two adult baboons (*P. papio*) weighing 25 kg (baboon 1) and 18 kg (baboon 2) were used. At the time of the experimentation the baboons were anesthetized with ketamine (10 mg per kilogram of body weight), paralyzed with gallamine, intubated with a cuffed endotracheal tube, and passively ventilated on a gas mixture of 70% nitrous oxide and 30% oxygen. To permit arterial blood sampling a small catheter was percutaneously placed in the femoral artery. To permit the intravenous injection of oxygen 15-labeled water, a small venous catheter was placed in the femoral vein.

The head of the baboon was positioned with the aid of a vertical laser line such that the center of the fifth slice (the PETT VI system provides seven simultaneous slices) corresponded to a line running transversely through the center of

the cerebral hemispheres. A lateral skull roentgenogram with the line marked by a vertical radiopaque wire provided a permanent record of the position and angulation for later correlation with anatomical observations (discussed later).

Attenuation was determined individually for each animal after positioning in PETT VI by obtaining a transmission scan using a ring source of activity (germanium 68) fitted to the PETT VI tomograph as previously described. Prior to the administration of [ $^{18}\text{F}$ ]spiperone, regional cerebral blood flow and regional cerebral blood volume were measured in baboon 1 by PET following the sequential administration of  $\text{H}_2^{15}\text{O}$  and  $\text{C}^{15}\text{O}$ . Measurement of regional cerebral blood flow and blood volume in baboon 2 was done on a day separate from the [ $^{18}\text{F}$ ]spiperone study. The lateral skull roentgenograms provided for accurate repositioning of the animal's head in the PET scanner.

Carrier-added [ $^{18}\text{F}$ ]spiperone was prepared by  $^{18}\text{F}$ -for- $^{19}\text{F}$  aromatic nucleophilic substitution, using spiperone and non-carrier-added fluorine 18-labeled tetrabutylammonium fluoride [16]. The [ $^{18}\text{F}$ ]spiperone, dissolved in a weakly acidic normal saline solution, was injected intravenously (baboon 1, 0.40 mg, 9.75 mCi/mg; baboon 2, 0.53 mg, 4.9 mCi/mg). Beginning with the administration of [ $^{18}\text{F}$ ]spiperone, arterial blood sampling was begun at a rate of one sample every 5 seconds and gradually tapered to a rate of one every 15 minutes near the end of the 2½-hour study. Samples were approximately 0.2 to 0.3 ml and were collected in pre-weighed 3 cc syringes. Actual volume was calculated by the difference in dry to wet weights assuming a specific gravity for blood of  $1.05 \text{ gm} \cdot \text{ml}^{-1}$ . Total activity was measured in a calibrated well counter.

PET scanning was done repeatedly over the length of the study, with scan lengths ranging from 2 minutes to 20 minutes. The longer scans at later times were necessary to achieve comparable counting statistics at the end of the study in the face of decaying and redistributing tracer. Total coincidence counts ranged from 300,000 to 1,200,000 per slice. Results were expressed as tissue activity at the midpoint of the PET scan.

To determine the underlying brain structure of the PET slices, baboon 1 was killed after the scan and the brain removed. After formalin fixation the brain was frozen in dry ice, partially thawed, and then sliced into 3.5 mm thick sections in the same planes as the PET study, using the lateral skull film taken at the time of the PET scan as reference. Brain slices were selected and photographed. The cerebellum and striatum were easily identified, and regions were then

placed on the PET scan slices to sample from these areas of interest.

To demonstrate the effect of specific binding site saturation on image contrast, baboon 2 underwent a second [ $^{18}\text{F}$ ]spiperone study two weeks after the first injection using additional spiperone carrier to achieve a higher molar dose and lower specific activity (12.0 mg, 0.10 mCi/mg). Values for CBF and CBV were obtained by PET as described on a day separate from the high-dose [ $^{18}\text{F}$ ]spiperone study. In an attempt to re-create the same physiological state, the animal was injected with unlabeled spiperone (12 mg) 30 minutes prior to PET measurements of CBF and CBV. The lateral skull roentgenogram was used to achieve accurate repositioning in reference to the first study.

## Results

Simulation results of error sensitivity for both  $PS$  and  $f_2$  estimation in cerebellum and  $PS$ ,  $k_{-1}$ , and  $BP$  estimation in specific binding site areas are summarized in Table 2.

The anatomical sections and corresponding PET slices for baboon 1 are shown in Figure 2. The PET slices are from the last scan ( $T = 154$  minutes) after injection of [ $^{18}\text{F}$ ]spiperone in which maximum discrimination between receptor-rich and receptor-poor areas is seen. Regions are selected as shown for cerebellum and striatum. The most anterior regions encompassing the eyes are placed for visual comparison only and were not included in the modeling work. The increased uptake in the eyes is not surprising, however, because a large number of specific binding sites for spiperone has been shown to exist in the retina [30]. The whole blood activity curve for baboon 1 is shown in Figure 3. The time activity curves for the PET regions selected on baboon 1 are plotted in Figure 4.

Two PET scan slices from baboon 2 are shown in Figure 5. The first is a late image ( $T = 133$  minutes) after the first injection (high specific activity, low molar dose) of [ $^{18}\text{F}$ ]spiperone. The second is a late image ( $T = 117$  minutes) in exactly the same plane as the first image, but after the second injection (low specific activity, high molar dose) of [ $^{18}\text{F}$ ]spiperone. For direct visual comparison both images are normalized to the fraction of the injected dose. Note the dramatic de-

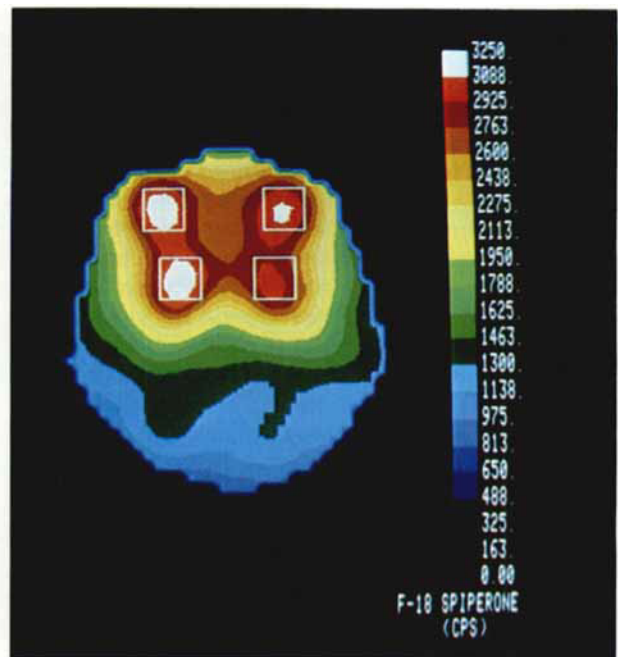
Table 2. Model Simulations

Starting Parameter	Percent Error Incurred by a +5% Change in Starting Parameter					
	$f_2$	$PS$	$k_{-1}$	$k'_1$	$BP$	
$F$	0.0	-1.3	-0.2	-0.4	-0.2	
$V_1$	-0.2	-0.3	-0.5	-0.7	-0.12	
$V_2$	-4.7	0.0	-10.4	-11.0	-1.7	
$f_1$	-5.0	-5.0	21.0	24.0	2.1	
$f_2$	...	...	16.0	14.0	-2.8	

The parameters used in these simulations are defined in Table 1 and the text (Methods section).



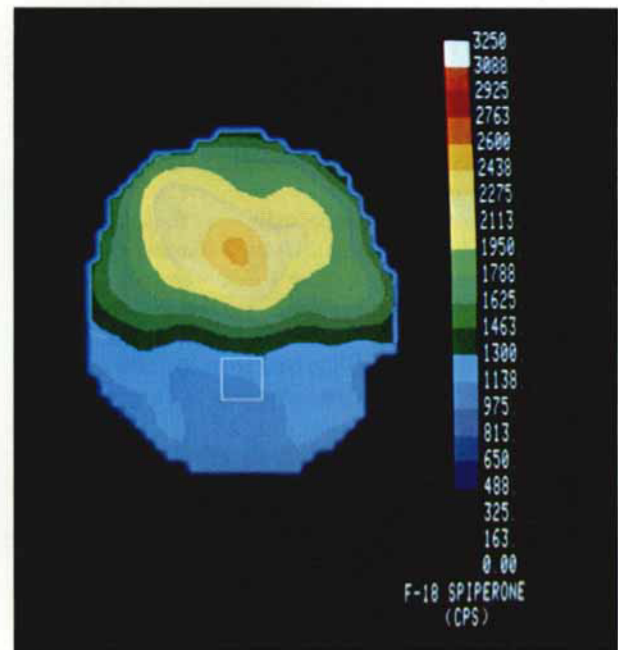
A



B



C



D

Fig 2. Baboon brain positron emission tomographic (PET) images (right) obtained after injection of  $^{18}\text{F}$ spiperone, shown with corresponding anatomical sections (left) obtained from the same animal postmortem. PET images were collected simultaneously (delay after injection was 154 minutes), decay corrected, and displayed as tissue activity (cps/ml). Bottom slices (C,D) are 1.4 cm more caudal than top slices. Square regions on the PET images demonstrate where data was obtained for cerebellum (D, single region) and striatum (B, posterior regions) for interpretation by the drug binding model. Regions over the retinal areas (B, anterior regions) are for visual comparison only. These same PET regions are also superimposed over the anatomical slices (A,C) for demonstration of the actual underlying anatomy.

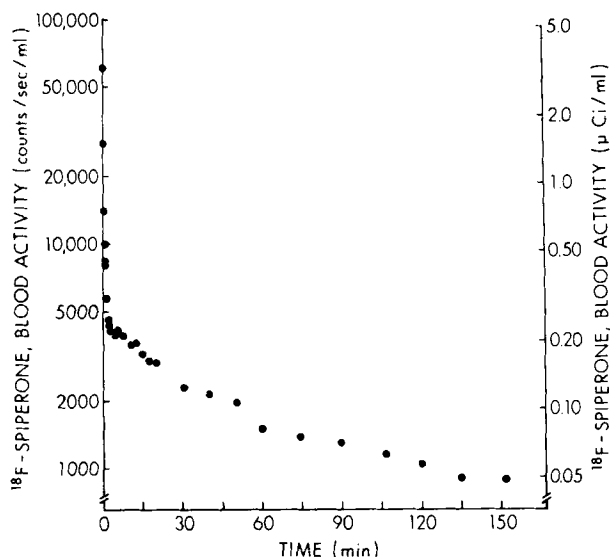


Fig 3. Semi-log plot of whole blood activity after intravenous injection of [ $^{18}\text{F}$ ]spiperone (dose; 0.40 mg, 9.75 mCi/mg). Each point represents one measurement and is decay corrected to time of injection.

crease in image contrast in the second image. This change appears to be a direct result of the greatly decreased fractional binding in the areas thought to be rich in specific binding sites.

Analysis with the receptor model was performed on the data sets resulting from all three injections of [ $^{18}\text{F}$ ]spiperone, and the findings are summarized in Table 3. However, the data from the second study on baboon 2 (high molar dose, low specific activity) had insufficient differences between striatum and cerebellum tissue activity curves to find mathematically unique solutions for receptor terms regardless of equation set used. For the data sets obtained from baboon 1 and after the first injection of baboon 2, the use of Eq. set 1 yielded only nonunique solutions of  $k_1$  and  $B_{\text{max}}$ . Thus, all receptor values are derived using Eq. set 2. The computer-generated curve-fit results from baboon 1 are plotted against the PET data in Figure 4.

## Discussion

### Technical Considerations

Evaluation of our proposed model should begin with consideration of assumptions inherent in its structure.

No provision is made for products of spiperone metabolism in the model. The presence of such compounds in the brain tissue could cause significant errors in data interpretation. Kuhar and colleagues [17], however, report no significant metabolism of spiperone in rat brain up to 2 hours after intravenous administration. Additionally, if spiperone metabolism were shown to occur in other organ systems (e.g., enterohepatic), the model would be unaffected unless the

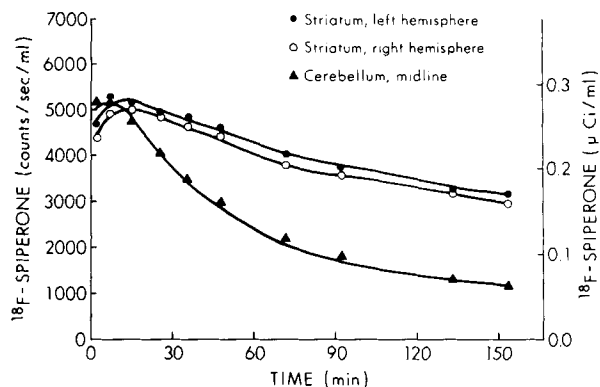
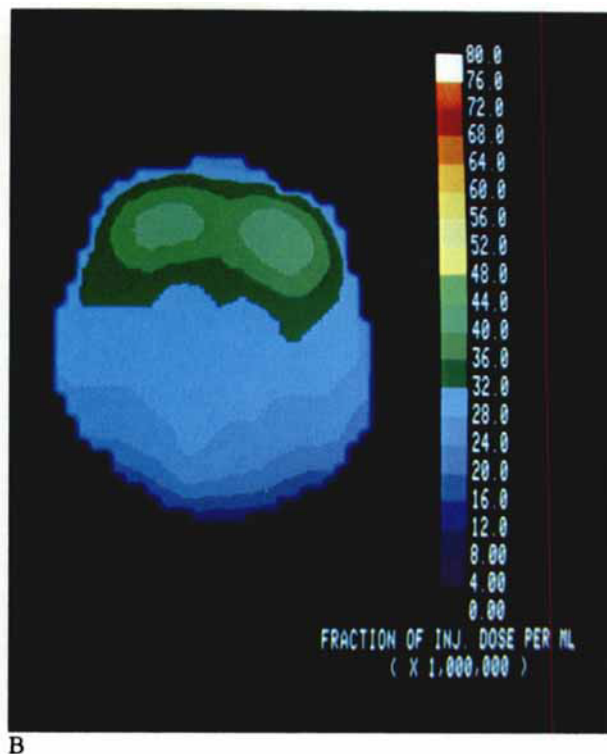
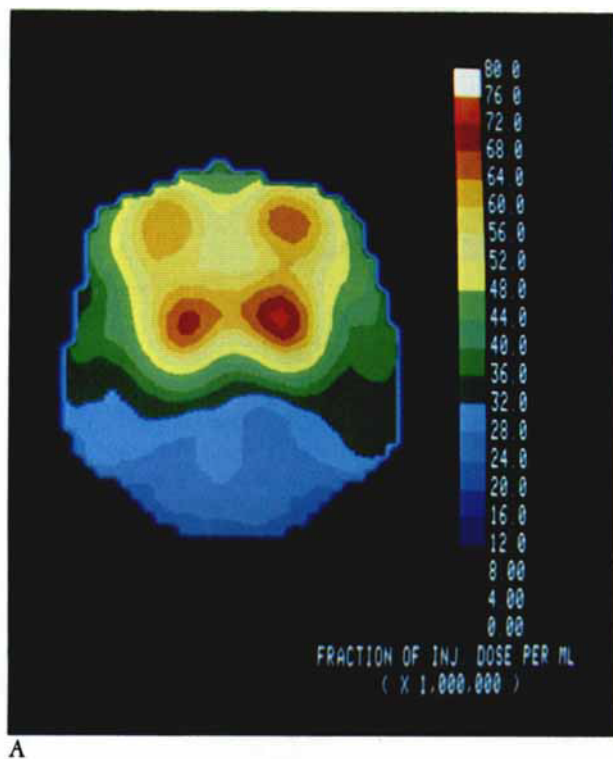


Fig 4. Regional tissue activity curves for three areas of the baboon brain after intravenous injection of [ $^{18}\text{F}$ ]spiperone. Each point represents the decay-corrected local tissue activity as measured by a positron emission tomographic image. The solid lines represent the best computer curve fit generated by the drug binding model.

metabolites entered the vascular system in significant quantities. Further work is required to assure that drug metabolism does not interfere with the model, but it should be done using [ $^{18}\text{F}$ ]spiperone. Other radiolabels may behave differently (e.g., hydrolysis of the label can affect tritium-labeled spiperone), and the results would not be applicable.

Nonspecific binding may confuse the interpretation of receptor binding data. Hartley and Seeman [10] demonstrate that a large error occurs with in vitro dopamine receptor characterization with spiperone when nonspecific binding is ignored. Generally, separation of the effects of nonspecific binding from those of specific receptor binding with in vitro studies requires a broad range of substrate concentrations, including levels that saturate all specific binding sites. This requirement would be impossible to meet in human in vivo studies, however, without producing unwanted pharmacological effects. Thus, the proposed model estimates nonspecific binding from the cerebellum, a brain tissue believed to have no specific binding sites for spiperone [17, 19]. This value is used to evaluate specific binding sites in all other brain tissues.

Only indirect evidence suggests spiperone nonspecific binding is constant throughout the brain. Kuhar and colleagues [17] and Laduron and co-workers [18, 19] have shown that as spiperone specific binding sites become saturated with increasing drug concentrations, total spiperone binding in rat striatum and in cerebellum become comparable. This technique, however, has not been applied systematically to investigate nonspecific binding throughout the brain. Nonspecific binding sites are most likely situated on many types of common cellular and structural proteins, however. To postulate the existence of regional changes in nonspecific binding, one would have to assume significant regional variations in the gross protein



makeup of brain tissue. Such variations seem unlikely in gray matter in different areas.

We assume that transport of spiperone out of the vascular space and into the tissues occurs through passive diffusion. The data from the studies of baboons and the associated modeling support such a mechanism in that the curve fit was close for all tissues at early time points, when transport plays a large role in determining tissue activity. Even if other transport mechanisms existed, with the tracer quantities of drug we propose for human studies, such systems would behave in a linear fashion and be indistinguishable from passive diffusion.

An important feature of our model is that we estimate the value for  $PS$ , the brain permeability–surface area product, for spiperone locally. This approach circumvents errors that would occur from extrapolating values for  $PS$  obtained, for example, from the cerebellum to the striatum, based on the evidence that capillary surface changes regionally throughout the brain [12, 31].

Certain pharmacological complexities of drug receptors are ignored in our model. For example, no provision is made for competition by endogenous neurotransmitters on receptor binding sites. We believe that this is a minor point, because it is doubtful that in normal animals or human subjects a large number of receptor sites are consistently tied up over the length of the study. Also, the very high affinity of spiperone compared with that of the major neurotransmitter, dopamine, reduces potential effects from competition for sites [26].

*Fig 5. Comparison of baboon brain positron emission tomographic images obtained with intravenous injection of  $^{18}\text{F}$ spiperone using (A) low molar dose, high specific activity (dose; 0.53 mg, 4.9 mCi/mg) and (B) high molar dose, low specific activity (dose; 12.0 mg, 0.10 mCi/mg). The images are of the same animal at the same level, angulation, and delay after injection (A, 133 minutes; B, 117 minutes). Both images have been corrected for decay and normalized to fraction of injected dose. Areas of increased drug binding are easily distinguishable in image A, but are dramatically diminished in image B. This effect is presumably the result of saturation of the specific binding sites with injection of the high molar doses.*

Our model does not attempt to describe a more precise receptor compartment than the extravascular tissue space. Although this may seem to be an oversimplification considering the knowledge that exists regarding cellular distribution, orientation to membranes, and possible sequestration of receptors in vesicles [18, 26, 29], including all of these factors would not change the behavior of the model as long as the ligand spiperone freely passes into all areas. Because the observed receptor kinetics proceed much more slowly than the transport across the blood-brain barrier and we assume that no membrane exists in the tissue with less permeability than that barrier, it is reasonable to conclude that spiperone can distribute homogeneously in the tissue space. Thus, despite a certain inhomogeneity of receptor distribution on the microscopic level, we believe that no additional refinements are needed presently in the model.



Table 3. Regional Parameter Values

Animal Study	Spiperone Dose (mg)	Supplied Parameters		Estimated Parameters by Model			
		$F$	$V_1$	$f_2$	$PS$	$k_{-1}$	$BP$
Baboon 1	0.40						
Cerebellum		0.012	0.060	0.058	0.032	...	
Striatum, left		0.012	0.057	...	0.028	$1.42 \times 10^{-4}$	21.6
Striatum, right		0.011	0.061	...	0.025	$1.35 \times 10^{-4}$	19.7
Baboon 2 (first study)	0.53						
Cerebellum		0.014	0.059	0.048	0.024	...	
Striatum, left		.015	0.046	...	0.028	$4.01 \times 10^{-4}$	17.4
Striatum, right		0.016	0.049	...	0.030	$3.98 \times 10^{-4}$	19.1
Baboon 2 (second study)	12.0						
Cerebellum		0.008	0.053	0.047	0.036	...	...
Mean $\pm$ SD		0.013 $\pm$ 0.003	0.055 $\pm$ 0.006	0.051 $\pm$ 0.006	0.029 $\pm$ 0.004	$2.7 \times 10^{-4}$ $\pm$ $1.5 \times 10^{-4}$	19.4 $\pm$ 1.73

See Table 1 for description of variables and units.  
SD = standard deviation.

Because of the well-known limitations of PET in spatial (approximately 1 cm<sup>3</sup>) and temporal (approximately 1 minute) resolution, use of our receptor model with PET data requires special comment.

Partial volume averaging necessitated by limited spatial resolution should always be considered a potential source of error. Selection of region(s) for cerebellum in the baboon was done accurately in our study with the aid of anatomical sections. Fortunately, the cerebellum in humans is sufficiently large that with extant anatomical reference techniques (e.g., lateral skull films, computed tomographic scanning in the plane of the PET slices), the problem of in vivo localization of this structure should be minimal. Regions selected for receptor analysis may be somewhat more difficult to localize because they are smaller. Additionally, these regions may be heterogeneous with respect to receptor type (two or, possibly, three types of dopamine receptors are believed to exist). The resultant  $BP$  will be a weighted linear average or, possibly, a nonlinear combination. The extensive simulations needed to demonstrate the nature of this averaging effect have not yet been done. A region containing nonbrain tissue (e.g., cerebrospinal fluid) should exhibit a significant nonlinear error in receptor characterization. A clue that such an error exists in the data would be an accompanying change in the  $PS$ , because the region would include tissue with a radically different degree of vascularity.

Limited temporal resolution may be especially important in describing the very early tissue activity curve. A PET scan can give only the integrated activity curve during the scan, not instantaneous activity, as required by the model. Currently we assume constant radioactivity during the scan and divide the accumulated PET activity (counts) by the scan length to estimate an instantaneous counting rate at the midpoint

of the scan. At early times the flux of radiotracer within the tissue may invalidate this assumption and lead to errors in model parameters, particularly  $PS$ . We see two possible approaches to this problem. The first, and easier, is to use a higher injected dose of radioactivity and scan for shorter times to obtain statistically valid results. This approach is severely limited by the restrictions on radiation dosage in human subjects, however. Another approach is to integrate the model equations twice. The second integration over the time of the scan allows the model to predict and compare directly the integrated tissue activity with the PET activity. We have successfully employed this technique in models for the measurement of CBF and CBV with PET [9, 25].

Our simulations (see Table 2), admittedly limited in scope, indicate that quantitative characterization of spiperone binding sites in terms of the binding potential is not critically dependent on the estimates of local blood flow, blood volume, and tissue nonspecific binding. Errors in local blood flow or blood volume estimation have surprisingly little effect on  $BP$  or the kinetic rate constants  $k_{-1}$  and  $k_1$ . A 5% error in the estimate of tissue nonspecific binding ( $f_2$ ) causes only a 2.8% error in  $BP$ , whereas large errors, 14% and 16%, were observed in the separate kinetic rate constants. This same pattern of differential sensitivity is seen when the error is placed in the blood nonspecific binding ( $f_1$ ) or the tissue volume ( $V_2$ ). In general the kinetic values are much more sensitive to errors in parameters other than  $BP$ . This bodes well for the use of the  $BP$  parameter in clinical investigation.

#### Biological Considerations

The data from our studies of baboons, obtained using [<sup>18</sup>F]spiperone and PET scanning, provide a truly

in vivo, quantitative representation of spiperone distribution and binding kinetics. Our parameter estimation strategy was successful when high-specific-activity [ $^{18}\text{F}$ ]spiperone was used. Low-specific-activity [ $^{18}\text{F}$ ]spiperone yielded data that could not be interpreted uniquely in terms of specific binding. This pattern will occur whenever specific binding in the tissue is low in relation to nonspecific binding. This situation can arise when large molar doses of unlabeled ligand are administered in conjunction with the radiolabeled ligand, as was done in our experiment. Under these circumstances most of the available specific binding sites are occupied by unlabeled ligand, a condition that should not occur in human studies because of the unwanted side effects of such high doses of a potent ligand. This situation can also arise, however, when a radioligand with a much lower specific binding affinity, relative to its nonspecific binding affinity, is used. A drastic reduction in either affinity or number of receptors resulting from a specific disease process could produce the same result.

Measurements of the brain permeability of spiperone, expressed as the product of permeability and capillary surface area, or  $PS$ , and determinations of whole tissue nonspecific binding have not been previously published, to our knowledge. Our value for the brain  $PS$  of spiperone ( $0.029 \text{ cm}^3 \cdot \text{sec}^{-1} \cdot \text{ml}^{-1}$ ) is quite similar to the brain  $PS$  for water (approximately  $0.021 \text{ cm}^3 \cdot \text{sec}^{-1} \cdot \text{ml}^{-1}$ ) previously measured in our laboratory [7, 24]. This similarity implies that a considerable percentage of the administered dose of labeled spiperone freely enters brain. Our data, however, indicate that only a small fraction of the administered dose actually reaches the brain tissue, probably because a large fraction (about 90%) of the labeled plasma spiperone is bound to plasma protein.

Spiperone specific binding characteristics have been studied extensively with in vitro techniques. The total number of binding sites ( $B_{\text{max}}$ ) has been estimated at values ranging from 0.76 nM to 12.75 nM in human striatum [20] and 16 nM to 28 nM in rat striatum [1, 27]. Values for  $K_D$  range from 0.14 nM to 0.39 nM in rat striatum [1, 27]. Thal and colleagues [29], studying spiperone binding in monkey caudate nucleus, report a  $B_{\text{max}}$  of 17.8 nM and a  $K_D$  of 1.1 nM. If these values are converted to our binding potential value, where  $BP = B_{\text{max}}/K_D$ , we find a range of 2.0 to 91.0 for human striatum (using the  $K_D$  values from the rat, because none are available for humans), 41 to 200 for rat striatum, and 16.2 for monkey caudate nucleus. Our in vivo values of  $BP$  (mean, 19.4) compare quite favorably, considering the range of results in the literature.

We wish to emphasize that the term *binding potential* ( $BP$ ) is more than a mathematical rearrangement of parameters. Its existence stems from the realization that with the administration of any radioligand in tracer

quantities, *no* in vivo model can separate the receptor's forward rate constant from the concentration of receptor sites. Without a priori assumptions regarding regional receptor kinetics, these terms must be lumped together as a product. Thus, with our model we obtain values for  $k_1 \cdot B_{\text{max}}$ , or  $k'_1$  and the reverse rate constant,  $k_{-1}$ . It was unclear to us how these two kinetic parameters ( $k'_1$  and  $k_{-1}$ ) could be related intuitively to possible brain pathophysiological mechanisms. We choose, therefore, to combine the two parameters by dividing  $k'_1$  by  $k_{-1}$ . This yields a parameter (i.e., the binding potential, or  $BP$ ) that is, quite simply, the total number of binding sites or receptors multiplied by their affinity for the ligand. As a result, we have a term that is linearly related to receptor concentration *and* to the receptor affinity for the ligand. As such, it should accurately reflect the potential of a specific membrane to interact with either a specific radioligand or, more important, a specific neurotransmitter (e.g., dopamine). A further feature of this parameter is that it has no units.  $BP$  also is easily shown to be the equilibrium ratio between receptor-bound ligand and free ligand. Thus, for any amount  $L$  of free neurotransmitter or radioligand, the product of  $BP$  and  $L$  is the maximum amount of receptor that will bind with the compound. This last characteristic is the basis for the name *binding potential*.

The reverse rate constant, or the fraction of bound ligand leaving the receptor per unit time,  $k_{-1}$ , has been estimated by Sundermann and Wooten [27] to be  $1.6 \times 10^{-3} \text{ sec}^{-1}$  in rat striatum. Our in vivo results for  $k_{-1}$  (mean,  $2.7 \times 10^{-4} \text{ sec}^{-1}$ ) in baboon striatum are lower by a factor of six. This difference, if not merely representative of the natural range of values for the different species, is most likely a result of the difference in measurement techniques. The in vitro method involves the creation of a membrane homogenate with an assuredly different chemical and stereotypical receptor environment. Our in vivo technique preserves the receptor environment and may be influenced by such hypothetical factors as receptor-receptor interactions that can decrease the "off rate." For these reasons in vivo techniques such as the one proposed here not only may provide data different from in vitro studies but may prove superior to in vitro techniques in accurately characterizing drug-receptor kinetics in living humans.

The next step is to apply our receptor model to [ $^{18}\text{F}$ ]spiperone PET data from human subjects. Work is under way to achieve routinely specific activities greater than 200 mCi/mg in the preparation of [ $^{18}\text{F}$ ]spiperone, thus allowing injection of 20 mCi with a dose of spiperone less than 0.1 mg, which should be devoid of acute pharmacological effects [21, 22]. Once this goal is achieved, we believe there will be no major obstacle to quantitative regional in vivo drug binding studies of the human brain.

## References

1. Akiyama K, Sato M, Otsuki S: Increased  $^3\text{H}$ -spiperone binding sites in mesolimbic area related to methamphetamine-induced behavioral hypersensitivity. *Biol Psychol* 17:223-231, 1982
2. Aoki M: Introduction to Optimization Techniques: Fundamentals and Application of Nonlinear Programming. New York, Macmillan, 1971, pp 99-115
3. Boyce WE, DePrima RE: Elementary Differential Equations. New York, Wiley, 1969, pp 328-368
4. Campbell A, Herschel M, Cohen BM, Baldessarini RJ: Tissue levels of haloperidol by radioreceptor assay and behavioral effects of haloperidol in the rat. *Life Sci* 27:633-640, 1980
5. D'Ambrosio A, Zivkovic B, Bartholini G: [ $^3\text{H}$ ]Haloperidol labels brain dopamine receptors after its injection into the internal carotid artery of the rat. *Brain Res* 238:470-474, 1982
6. Eckelman WC (ed): Receptor-binding Radiotracers, Vol 1. Boca Raton, FL, CRC Press, 1982, p 105
7. Eichling JO, Raichle ME, Grubb RL, et al: Evidence of the limitations of water as a freely diffusible tracer in the brain of the rhesus monkey. *Circ Res* 35:358-364, 1974
8. Fowler JS, Arnett CD, Wolf AP, et al: [ $^{11}\text{C}$ ]Spiroperidol: synthesis, specific activity determination, and biodistribution in mice. *J Nucl Med* 23:437-445, 1982
9. Grubb RL Jr, Raichle ME, Higgins CS, Eichling JO: Measurement of regional cerebral blood volume by emission tomography. *Ann Neurol* 4:322-328, 1978
10. Hartley EJ, Seeman P: The effect of varying  $^3\text{H}$ -spiperone concentration on its binding parameters. *Life Sci* 23:513-518, 1978
11. Herscovitch P, Markham J, Raichle ME: Brain blood flow measured with intravenous  $\text{H}_2^{15}\text{O}$ . I. Theory and error analysis. *J Nucl Med* 24:782-789, 1983
12. Hertz MM, Paulson OB: Transfer across the human blood-brain barrier: evidence for capillary recruitment and for a paradox glucose permeability increase in hypocapnia. *Microvasc Res* 24:364-376, 1982
13. Katzman R, Pappius HM: Brain Electrolytes and Fluid Metabolism. Baltimore, Williams & Wilkins, 1973, p 5
14. Kety SS: The theory and application of the exchange of inert gas at the lungs and tissues. *Pharmacol Rev* 3:1-41, 1951
15. Kety SS: Measurement of local blood flow by the exchange of an inert, diffusible substance. *Methods Med Res* 8:228-236, 1960
16. Kilbourn MR, Welch MJ, Dence CS, et al: Carrier-added and no-carrier-added syntheses of [ $^{18}\text{F}$ ]spiroperidol and [ $^{18}\text{F}$ ]haloperidol. *Int J Appl Rad Isot* (in press)
17. Kuhar MJ, Murrin LC, Malouf AT, Klemm N: Dopamine receptor binding in vivo: the feasibility of autoradiographic studies. *Life Sci* 22:203-210, 1978
18. Laduron PM, Janssen PFM, Leysen JE: Spiperone: a ligand of choice for neuroleptic receptors. II. Regional distribution and in vivo displacement of neuroleptic drugs. *Biochem Pharmacol* 27:317-321, 1978
19. Laduron P, Leysen J: Specific in vivo binding of neuroleptic drugs in rat brain. *Biochem Pharmacol* 26:1003-1007, 1977
20. Mackay AVP, Doble A, Bird ED, et al:  $^3\text{H}$ -Spiperone binding in normal and schizophrenic post-mortem human brain. *Life Sci* 23:527-532, 1978
21. Matthe DJ: A pilot investigation in neuroleptic therapy. *Dis Nerv Sys* 29:515-524, 1968
22. Nomura H: Clinical experience with spiperone. *Clin Med* 10:3-10, 1973
23. Raichle ME: In vivo autoradiography with positron emission tomography. *Brain Res Rev* 1:47-68, 1979
24. Raichle ME, Eichling JO, Straatmann MD, et al: Blood brain permeability of  $^{11}\text{C}$ -labeled alcohols and  $^{15}\text{O}$ -labeled water. *Am J Physiol* 230:543-552, 1976
25. Raichle ME, Martin WRW, Herscovitch P, et al: Brain blood flow measured with intravenous  $\text{H}_2^{15}\text{O}$ . II. Implementation and validation. *J Nucl Med* 24:790-798, 1983
26. Seeman P: Brain dopamine receptors. *Pharmacol Rev* 32:229-313, 1981
27. Sundermann RH, Wooten GF: Biochemical properties of spiperone binding to rat brain membranes. *Pharmacology* 21:295-305, 1980
28. Ter-Pogossian MM, Ficke DC, Hood JT, et al: PETT VI: a positron emission tomography utilizing cesium fluoride scintillation detectors. *J Comput Assist Tomogr* 6:125-133, 1982
29. Thal LJ, Makman MH, Ahn HS, et al:  $^3\text{H}$ -Spiroperidol binding and dopamine-stimulated adenylate cyclase: evidence for multiple classes of receptors in primate brain regions. *Life Sci* 23:629-634, 1978
30. Watling KJ, Iversen LL: Comparison of the binding of [ $^3\text{H}$ ]spiperone and [ $^3\text{H}$ ]domperidone in homogenates of mammalian retina and caudate nucleus. *J Neurochem* 37:1130-1143, 1981
31. Weiss HR, Buchweitz E, Murtha TJ, Auletta M: Quantitative regional determination of morphometric indices of the total and perfused capillary network in the rat brain. *Circ Res* 51:494-503, 1982
32. Wilde DJ, Beightler CS: Foundations of Optimization. Englewood Cliffs, NJ, Prentice-Hall, 1967, pp 304-313
33. Yamamoto MM, Ficke DC, Ter-Pogossian MM: Performance study of PETT VI, a positron computed tomograph with 288 cesium fluoride detectors. *IEEE Trans Nucl Sci* NS-29:529-533, 1982